2023 European Control Conference (ECC)
June 13-16, 2023. Bucharest, Romania

Cooperative control of multi-tilt tricopter drones applying a 'mixed' negative imaginary and strict passivity technique

Daniel Abara, Parijat Bhowmick, *Member, IEEE*, and Alexander Lanzon, *Senior Member, IEEE*

***Abstract*— This paper develops a cooperative controller for a fleet of multi-tilt tricopter drones modelled as Negative Imaginary (NI) systems via closed-loop linearisation exploiting Sliding-Mode Control (SMC) technique. The multi-tilt tricopter model is derived from the first principles, and the SMC method is invoked to obtain a closed-loop linear model of the tricopter plant with six outputs and six inputs. A subspace-based system identification algorithm is developed to identify the linearised drone model enforcing the NI property. The primary control objective is to design a distributed 'mixed' NI and strictly Passive control protocol so that the tricopter agents asymptotically reach the desired formation and keep tracking the target. Instead of the Lyapunov approach, the characteristic loci method is used to prove the asymptotic convergence of the trajectory tracking error. Finally, an exhaustive simulation case study is carried out on a fleet of six multi-tilt tricopter drones to demonstrate the feasibility of the cooperative controller presented in this work.**

I. Introduction

Cooperative control of UAVs (e.g. quadcopters, tricopters) has drawn the importance of academia and industry due to their widespread applications in reconnaissance [1], search and rescue [2], inspection and mapping [3], target localisation and tracking, precision agriculture, etc. Commercial drones have become more efficient, reliable, compact in size, durable, and offer longer flight time and higher payload capacity with the advent of modern gyroscopes and accelerometers, high-speed embedded processors and high-power batteries. Different from the classic quadcopter, where the three dimensional position tracking is indirectly accomplished by controlling the attitude, multi-tilt tricopters can attain attitude and position control independently and simultaneously (complete 6-DOF control) due to their airframe. This means that, multi-tilt tricopters (or simply *tricopters*) overcome the limitations of the classic quadcopter in this regard, and translation in the x and y directions can be achieved without modifying the attitude (roll, pitch and yaw angles). This paper aims to design a simple yet effective cooperative controller for a group of networked tricopter drones utilising the NI theory, characteristic loci technique and SMC-based linearisation principles. Negative Imaginary (NI) systems theory has attracted the interest of control theorists and practising engineers due to its potential to solve various real-life engineering challenges, like vibration control of lightly-damped systems [4], cantilever beams [5], [6]; nano-positioning applications [7]; cooperative train platooning [8]; control of dissipative systems [9]–[11]; etc. Due to a simple robust stability criterion depending only on the loop gain at zero frequency (known as the *DC loop gain* condition [4]), NI theory has gained a lot of traction. In a SISO setting, an NI transfer function's imaginary part remains negative for all $\omega \geq 0$. Among the strict subclasses within the NI class, Strictly NI (SNI [4]) and Output Strictly NI (OSNI [9], [12]–[14]) appear frequently in the literature. The primary motivation for applying NI theory in this work is that a certain class of tricopter drones may be converted into (or modelled as) an NI system in closed loop via feedback linearisation or SMC-based linearisation and hence, a network of such tricopters can then be controlled by a distributed SNI controller. This idea deploys the cooperative control scheme as the outer-loop controller while the SMC-based linearising control law works in the inner loop. The article [15] has proceeded along this direction and offered significant contributions on designing a cooperative control scheme for quadrotor UAVs. In this paper, we have used an SMC-based linearisation technique in contrast to the feedback linearisation technique (used in [16] for the same purpose) since the latter lacks in preserving robustness properties due to relying on the inverse-based nonlinearity cancellation. To describe the linearised tricopter closed-loop system as an NI system (the inner-loop), a subspace-based closed-loop identification algorithm is developed to guarantee that the resulting model is NI. A distributed SNI controller based on output-feedback is then proposed to guarantee formation tracking for a group of tricopter drones. To prove stability and show that the tracking error (which includes both formation and cooperative tracking) converges, we utilize a new approach that uses the features of the characteristic loci from a network of SNI and NI plants rather than commonly used Lyapunov methods.

This work was supported by the Nigerian Petroleum Technology Development Fund (PTDF), the Engineering and Physical Sciences Research Council (EPSRC) [grant number EP/R008876/1] and by the Science and Engineering Research Board (SERB), DST, India [grant number SRG/2022/000892]. All research data supporting this publication are directly available within this publication.

D. Abara is with Quanser Consulting Inc., Markham, Canada, D. Abara & A. Lanzon are with the Department of EEE, School of Engineering, University of Manchester, Manchester M13 9PL, UK., and P. Bhowmick is with the Department of EEE, IIT Guwahati, Assam - 781039, India. Emails: Daniel.Abara@quanser.com, Daniel.Abara@manchester.ac.uk, parijat.bhowmick@iitg.ac.in, Alexander.Lanzon@manchester.ac.uk.

II. Essential preliminaries

A. Coordinate rotations

Using the Euler z, y, x rotation sequence [17], a body may be transformed from the earth frame (which is inertial) to

body-fixed frame using the following rotation matrix

$$\boldsymbol{R}_e^b(\boldsymbol{\eta}) = \begin{bmatrix} c_\theta c_\psi & c_\theta s_\psi & -s_\theta \\ s_\phi s_\theta c_\psi - c_\phi s_\psi & s_\phi s_\theta s_\psi + c_\phi c_\psi & s_\phi c_\theta \\ c_\phi s_\theta c_\psi + s_\phi s_\psi & c_\phi s_\theta s_\psi - s_\phi c_\psi & c_\phi c_\theta \end{bmatrix}, \quad (1)$$

where $\boldsymbol{\eta} = [\phi\ \theta\ \psi]^\top$, $c_\phi = \cos\phi$ and $s_\phi = \sin\phi$. In similar fashion, the Euler angle rates may be transformed from the body to inertial frame using [17]

$$\boldsymbol{\Gamma} = \begin{bmatrix} 1 & \sin\phi\tan\theta & \cos\phi\tan\theta \\ 0 & \cos\phi & -\sin\phi \\ 0 & \sin\phi\sec\theta & \cos\phi\sec\theta \end{bmatrix}. \quad (2)$$

B. Passive and NI properties

This subsection includes the frequency-domain definitions of Passive and NI systems. We will first go through the definitions of Passive and Strictly Passive systems. Note that, for LTI systems, passive and Positive-real (PR) properties are equivalent. In fact, LTI passive systems are characterised by PR transfer functions.

Definition 1: (**Passive System**) [18] A system $\Sigma(s) \in \mathscr{R}^{m\times m}$ with no RHP poles is called Passive if $\Sigma(j\omega) + \Sigma(j\omega)^* \geq 0\ \forall\omega \in \mathbb{R}$ except those $\omega_0 \in \omega$ where $s = j\omega_0$ is a pole of $\Sigma(s)$. The multiplicity of the pole $s = j\omega_0$ cannot be more than one and the residue matrix $\Delta|_{s=j\omega_0} \triangleq \lim_{s\to j\omega_0}(s - j\omega_0)\Sigma(s) = \Delta|^*_{s=j\omega_0} \geq 0$.

Definition 2: (**Strictly Passive System**) [18] A system $\Sigma(s) \in \mathscr{RH}_\infty^{m\times m}$ is called strictly Passive if $\Sigma(j\omega) + \Sigma(j\omega)^* > 0\ \forall\omega \in \mathbb{R}$.

We will now cover NI and SNI definitions.

Definition 3: (**NI System**) [19] A system $\Sigma(s) \in \mathscr{R}^{m\times m}$ with no RHP poles is NI if $j[\Sigma(j\omega) - \Sigma(j\omega)^*] \geq 0$ for all $\omega \in (0, \infty)$ leaving out those $\omega_0 \in \omega$ in which $s = j\omega_0$ is a pole of $\Sigma(s)$. If $\omega_0 \in (0, \infty)$, the multiplicity of the pole $(s^2 + \omega_0^2)$ cannot be more than one and the residue matrix $\Delta|_{s=j\omega_0} \triangleq \lim_{s\to j\omega_0}(s - j\omega_0)j\Sigma(s) = \Delta|^*_{s=j\omega_0} \geq 0$. If a pole of $\Sigma(s)$ is $s = 0$, then $\lim_{s\to 0} s^k\Sigma(s) = 0$ for all $k \geq 3$ and the residue matrix $\Delta|_{s=0} \triangleq \lim_{s\to 0} s^2\Sigma(s)\Delta|^*_{s=0} \geq 0$.

Definition 4: (**SNI System**) [4], [19] A system $\Sigma(s) \in \mathscr{RH}_\infty^{m\times m}$ is SNI if $j[\Sigma(j\omega) - \Sigma(j\omega)^*] > 0\ \forall\omega \in (0, \infty)$.

C. Characteristic loci theory

The concept of *characteristic loci* and its application in determining closed-loop asymptotic stability of LTI MIMO systems were introduced during 1969–1973 by MacFarlane and Belletrutti [20]. This concept is analogous to a *multi-loop* Nyquist criterion that offers a pretty convenient graphical stability analysis tool for MIMO systems. The characteristic loci $\bar{\lambda}_i(s)$, where $i \in \{1, 2, \ldots, m\}$, of any square LTI system $\Sigma(s) \in \mathscr{R}^{m\times m}$ is a conformal transform of the complex function $\det[\Sigma(s)]$ into another complex (argand) plane when s follows the standard s-plane D-contour in a CW direction (see Fig. 4a).

Theorem 1: [20] The closed-loop interconnection of two LTI systems $\Sigma(s)$ and $\Sigma_c(s)$, connected via negative feedback, is asymptotically stable if and only if the total number of the CCW encirclements about the $(-1 + j0)$ point by the characteristic loci $\bar{\lambda}_i(j\omega)$ of $L(s) \triangleq \Sigma(s)\Sigma_c(s)\ \forall i \in \{1, 2, \ldots, n\}$ is equal to the number of Right-half plane poles of $L(s)$. When $L(s) \in \mathscr{RH}_\infty^{m\times m}$, none of the characteristic loci $\bar{\lambda}_i(j\omega)$ should encircle the $(-1 + j0)$ point.

D. Multi-agent NI and SNI systems

This paper has exploited the multi-agent NI theory for modelling and controlling a multi-tricopter system whose linearised (via an inner-loop sliding-mode controller) dynamics can be well fitted into a six-channel SNI system model. The interactions or communications among the agents are modelled by an algebraic graph $\mathscr{G}$, which is characterised by its Laplacian matrix $\mathscr{L}$.

Property 1: The communication topology $\mathscr{G}$ among the agents is undirected and there exists at least one root node (target or virtual leader) that has direct/indirect connection to all the agents in the network.

As a consequence of Property 1, the graph Laplacian matrix $\mathscr{L} = \mathscr{L}^\top \in \mathbb{R}^{N\times N}$ and the pinning-gain matrix $\mathbb{P}_G = \mathrm{diag}\{w_{0,1}, w_{0,2}, \cdots, w_{0,N}\} \in \mathbb{R}^{N\times N}$ hold the relationship $\mathscr{L} + \mathbb{P}_G > 0$. The first subscript '0' indicates the root node, which stands for the target or virtual leader or simply the reference generator. It is an exo-system that may have a dynamics independent of the dynamics of the agents. For the heterogeneous cases, the graph observes the property $\Re\{\lambda_i[\mathscr{L} + \mathbb{P}_G]\} > 0\ \forall i \in \{1, 2, \ldots, N\}$.

We will now review some fundamental properties of multi-agent NI systems. [21] first established that a homogeneous network of NI (or SNI) agents, given by $\bar{\Sigma}(s) = (\mathscr{L} + \mathbb{P}_G) \otimes \Sigma(s)$, retains the NI (or SNI) property and $\bar{\Sigma}(0) > 0$ (or < 0) $\Leftrightarrow \Sigma(0) > 0$ (or < 0). In recent times, [22] and [23] have derived a crucial property of a multi-agent NI system exploiting the results of [24]. It asserts that all the characteristic loci $\bar{\lambda}_i(j\omega)$ of a homogeneous multi-agent NI (or SNI) system lie in the union of the fourth and third complex plane quadrants (also known as the characteristic loci plane, discussed in Subsection II-C).

III. Tricopter modelling, linearisation and system identification

This section describes the modelling and linearisation of the tricopter drone. The model identification of the linearised tricopter while enforcing the NI constraints is also presented. The modelling part is inspired by [16] and [25].

A. Forces and moments

From Fig. 1, the total rotor force (equivalent force from the three rotors) in body-fixed coordinates [25] is given by $\mathbf{F}_m^b = \begin{bmatrix} f_x & f_y & f_z \end{bmatrix}^\top = \sum_{i=1}^3 \boldsymbol{f}_i^b = k_t\boldsymbol{\Psi}_t\boldsymbol{\Omega}$ where

$$\boldsymbol{\Psi}_t = \begin{bmatrix} -\frac{\sqrt{3}}{2} & \frac{\sqrt{3}}{2} & 0 & 0 & 0 & 0 \\ \frac{1}{2} & \frac{1}{2} & -1 & 0 & 0 & 0 \\ 0 & 0 & 0 & -1 & -1 & -1 \end{bmatrix}, \boldsymbol{\Omega} = \begin{bmatrix} \omega_1^2\sin\alpha_1 \\ \omega_2^2\sin\alpha_2 \\ \omega_3^2\sin\alpha_3 \\ \omega_1^2\cos\alpha_1 \\ \omega_2^2\cos\alpha_2 \\ \omega_3^2\cos\alpha_3 \end{bmatrix}.$$

From Fig. 1, let $\boldsymbol{G}_{o_i}\ \forall i \in \{1, 2, 3\}$ be the 3D distance of rotor i respectively from the tricopter's centre of mass, and

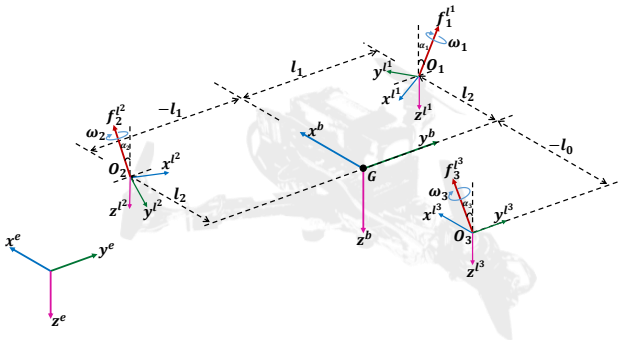

Fig. 1: Forces and moments acting on the tricopter.

$O_i\ \forall i \in \{1,2,3\}$ be the application points of $\boldsymbol{f}_i$ respectively, with $l_2 = \frac{1}{2}l_0$, $l_1 = \frac{\sqrt{3}}{2}l_0$ and l_0 being the arm length. Then, the total rotor torque in body-fixed coordinates [25] is given as $\mathbf{T}_r^b = \sum_{i=1}^{3}(\boldsymbol{G}_{o_i} \times \boldsymbol{f}_i^b) = k_t \boldsymbol{\Psi}_d \boldsymbol{\Omega}$ where

$$\boldsymbol{\Psi}_d = \begin{bmatrix} 0 & 0 & 0 & -l_1 & l_1 & 0 \\ 0 & 0 & 0 & l_2 & l_2 & -l_0 \\ l_0 & l_0 & l_0 & 0 & 0 & 0 \end{bmatrix}. \tag{3}$$

The drag torque produced as a result of each spinning propellers may be expressed in inertial coordinates as $\boldsymbol{\tau}_{d,i}^{l^i} = \begin{bmatrix} 0 & -k_d\omega_i^2 \sin\alpha_i & -k_d\omega_i^2\cos\alpha_i \end{bmatrix}^\top\ \forall i \in \{1,2,3\}$, and in body-fixed coordinates as $\boldsymbol{\tau}_{d,i}^b = \boldsymbol{R}_e^b(\boldsymbol{\eta})\boldsymbol{\tau}_{d,i}^{l^i}$. The total torque due to drag from the three rotors is thus $\mathbf{T}_d^b = \sum_{i=1}^{3}\boldsymbol{\tau}_{d,i}^b = k_d\boldsymbol{\Psi}_t\boldsymbol{\Omega}\ \forall i \in \{1,2,3\}$. The sum total of torques produced by the tricopter is therefore obtained as $\mathbf{T}_m^b = \mathbf{T}_r^b + \mathbf{T}_d^b = (k_t\boldsymbol{\Psi}_d + k_d\boldsymbol{\Psi}_t)\boldsymbol{\Omega} \in \mathbb{R}^3$. Hence, the tricopter's inputs $\mathbf{U} = \begin{bmatrix}\mathbf{F}_m^b & \mathbf{T}_m^b\end{bmatrix}^\top$ and actuator commands $\boldsymbol{\Omega}$ are related by the following expression

$$\mathbf{U} = \mathbf{M}\boldsymbol{\Omega} \tag{4}$$

where

$$\mathbf{M} = \begin{bmatrix} -\frac{\sqrt{3}}{2}k_t & \frac{\sqrt{3}}{2}k_t & 0 & 0 & 0 & 0 \\ \frac{1}{2}k_t & \frac{1}{2}k_t & -k_t & 0 & 0 & 0 \\ 0 & 0 & 0 & -k_t & -k_t & -k_t \\ -\frac{\sqrt{3}}{2}k_d & \frac{\sqrt{3}}{2}k_d & 0 & -\frac{\sqrt{3}}{2}k_t l_0 & \frac{\sqrt{3}}{2}k_t l_0 & 0 \\ \frac{1}{2}k_d & \frac{1}{2}k_d & -k_d & \frac{1}{2}k_t l_0 & \frac{1}{2}k_t l_0 & -k_t l_0 \\ k_t l_0 & k_t l_0 & k_t l_0 & -k_d & -k_d & -k_d \end{bmatrix}.$$

Remark 1: It can be shown that $\mathbf{M}$ is always full rank and invertible if $k_t, l_0 > 0$, as utilized in Fig.2.

B. Rigid-body model

From Newton-Euler modelling techniques [17], the tricopter dynamics is given as

$$\begin{bmatrix}\mathbf{F}_m^b \\ \mathbf{T}_m^b\end{bmatrix} = \begin{bmatrix}\boldsymbol{R}_e^b & 0 \\ 0 & \boldsymbol{I}_3\end{bmatrix}\left(\begin{bmatrix}m\boldsymbol{I}_3 & 0 \\ 0 & \mathbf{I}\end{bmatrix}\begin{bmatrix}\ddot{\boldsymbol{\xi}}^e \\ \dot{\boldsymbol{\omega}}^b\end{bmatrix} + \begin{bmatrix}\mathbf{F}_g^e \\ (\boldsymbol{\omega}^b \times \mathbf{I}\boldsymbol{\omega}^b)\end{bmatrix}\right), \tag{5}$$

and from (2)

$$\dot{\boldsymbol{\eta}} = \boldsymbol{\Gamma}\boldsymbol{\omega}^b, \tag{6}$$

where $\boldsymbol{\xi}^e$, $\boldsymbol{\omega}^b$, denote the 3D linear position and angular velocity respectively, $\boldsymbol{I}_3 \in \mathbb{R}^3$ is the identity matrix and $\mathbf{I} = \mathrm{diag}\{I_x, I_y, I_z\}$ is the inertia matrix.

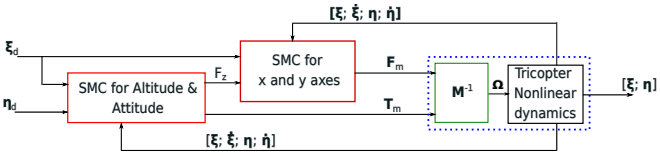

Fig. 2: SMC-based linearisation of the tricopter dynamics.

C. Linearisation using SMC

Assuming small angles for ϕ and θ, $\boldsymbol{\Gamma} \approx \boldsymbol{I}_3$ via (2). This implies $\ddot{\boldsymbol{\eta}} = \dot{\boldsymbol{\omega}}^b$ in (6) which when expanded yields

$$\ddot{\phi} = \big[\tau_\phi + (I_y - I_z)\dot{\theta}\dot{\psi}\big]/I_x, \tag{7}$$
$$\ddot{\theta} = \big[\tau_\theta + (I_z - I_x)\dot{\phi}\dot{\psi}\big]/I_y, \tag{8}$$
$$\ddot{\psi} = \big[\tau_\psi + (I_x - I_y)\dot{\phi}\dot{\theta}\big]/I_z. \tag{9}$$

Also, let us assume that for motion in z-axis (vertical motion), $\Sigma f_z \neq 0$, $\Sigma f_x = \Sigma f_y = 0$; for motion in x-axis, $\Sigma f_y = 0$, $\Sigma f_x \neq 0$, $\Sigma f_z \neq 0$; and for motion in y-axis, $\Sigma f_y \neq 0, \Sigma f_x = 0, \Sigma f_z \neq 0$. These assumptions are sensible since thrust is essential for motion in all axes (to maintain altitude), but f_x is mainly for motion in the x-axis while f_y is mainly for motion in the y-axis. Applying these assumptions to the translational dynamics from (5) results in

$$\ddot{x} = \big[(c_\phi s_\theta c_\psi + s_\phi s_\psi)f_z + (c_\theta c_\psi)f_x\big]/m, \tag{10}$$
$$\ddot{y} = \big[(c_\phi s_\theta s_\psi - s_\phi c_\psi)f_z + (s_\phi s_\theta s_\psi + c_\phi c_\psi)f_y\big]/m, \tag{11}$$
$$\ddot{z} = \big[(c_\phi c_\theta)f_z\big]/m + g. \tag{12}$$

Let us now define a sliding surface $\tilde{s}_\phi = \dot{e}_\phi + \lambda_\phi e_\phi$ for the roll dynamics (7) following [26], where λ_ϕ is positive and the roll angle error is $e_\phi = \phi - \phi_d$. If a reaching law $\dot{\tilde{s}} = -k_\phi\,\mathrm{sgn}(\tilde{s}_\phi)$, $k_\phi > 0$ is selected and a Lyapunov candidate $V_\phi = \frac{1}{2}\tilde{s}_\phi^2 > 0$ is considered for stability analysis, then

$$\dot{V}_\phi = \tilde{s}_\phi\dot{\tilde{s}}_\phi = -\tilde{s}_\phi k_\phi\,\mathrm{sgn}(\tilde{s}_\phi) = -k_\phi|\tilde{s}_\phi| \leq 0,$$

which implies

$$\tilde{s}_\phi\big(I_x^{-1}\big[(I_y - I_z)\dot{\theta}\dot{\psi} + \tau_\phi\big] - \ddot{\phi}_d + \lambda_\phi\dot{e}_\phi\big) = -k_\phi|\tilde{s}_\phi|,$$

and by rearranging

$$\tau_\phi = -I_x\big(k_\phi\,\mathrm{sgn}(\tilde{s}_\phi) + \lambda_\phi\dot{e}_\phi - \ddot{\phi}_d\big) - (I_y - I_z)\dot{\phi}\dot{\psi}$$

where $\mathrm{sgn}(\tilde{s}) = \dfrac{|\tilde{s}|}{\tilde{s}} = \begin{cases} -1, \tilde{s} < 0; \\ 0, \tilde{s} = 0; \\ 1, \tilde{s} > 0. \end{cases}$

It is evident that an equilibrium point exists at $\tilde{s}_\phi = 0$ and is asymptotically stable via [26] because V_ϕ is positive definite and the surface $\dot{\tilde{s}}_\phi$ satisfies $\dot{V}_\phi \leq 0$. Hence, the linearising input τ_ϕ will stabilize the roll angle. By using similar derivations in (8)–(12),

$$\tau_\theta = -I_y\big(k_\theta\,\mathrm{sgn}(\tilde{s}_\theta) + \lambda_\theta\dot{e}_\theta - \ddot{\theta}_d\big) - (I_z - I_x)\dot{\theta}\dot{\psi},$$
$$\tau_\psi = -I_z\big(k_\psi\,\mathrm{sgn}(\tilde{s}_\psi) + \lambda_\psi\dot{e}_\psi - \ddot{\psi}_d\big) - (I_x - I_y)\dot{\phi}\dot{\theta},$$

TABLE I: Tricopter parameters considered in this paper

Name of parameter	Value
Arm length l_0	0.330 m
Tricopter mass m	1.449 kg
Thrust constant k_t	0.1081×10^{-4} kg-m
Drag constant k_d	0.1729×10^{-6} kg-m^2
Inertia in x axis I_x	0.1037 kg-m^2
Inertia in y axis I_y	0.1031 kg-m^2
Inertia in z axis I_z	0.171 kg-m^2

$$f_x = -\frac{1}{c_\psi c_\phi}\big(m\big(k_x \operatorname{sgn}(\tilde{s}_x) - \ddot{x}_d + \lambda_x \dot{e}_x\big) - f_z(s_\psi s_\phi + c_\psi s_\theta c_\phi)\big),$$

$$f_y = -\frac{1}{(c_\psi c_\phi + s_\psi s_\theta s_\phi)}\big(m\big(k_y \operatorname{sgn}(\tilde{s}_y) - \ddot{y}_d + \lambda_y \dot{e}_y\big) - f_z(c_\phi s_\theta s_\psi - c_\psi s_\phi)\big),$$

$$f_z = -\frac{m}{c_\phi c_\theta}\big(k_z \operatorname{sgn}(\tilde{s}_z) + g - \ddot{z}_d + \lambda_z \dot{e}_z\big).$$

D. Tricopter model identification imposing NI constraints

A fairly accurate NI model of the linearised tricopter discussed in Section III-C, having six input-output channels with respect to the input variables x_d, y_d, z_d, ϕ_d, θ_d and ψ_d, needs to be identified in closed-loop. We collect data by passing a square wave as input to each channel and recording the output signal. The identification algorithm is described in [27] except that in our case, the estimation of the B matrix is done as a constrained optimization problem involving the NI property. The NI property has been embedded through the relationship $AY + YA^\top \leq 0$ and $B + AYC^\top = 0$ (referred to as the NI Lemma [4]). We have estimated the A and C matrices relying on the procedure in [27] and have obtained the following six transfer functions of the SMC-linearised tricopter model, which are stable NI.

$$\Sigma_1(s) = \frac{x}{x_d} = \frac{0.237 \times 10^{-4} s + 0.352 \times 10^{-4}}{s^2 + 0.00630 s + 0.436 \times 10^{-4}}, \quad (13)$$

$$\Sigma_2(s) = \frac{y}{y_d} = \frac{0.266 \times 10^{-13} s + 0.271 \times 10^{-4}}{s^2 + 0.00663 s + 0.368 \times 10^{-4}}, \quad (14)$$

$$\Sigma_3(s) = \frac{z}{z_d} = \frac{0.877 \times 10^{-13} s + 0.238 \times 10^{-4}}{s^2 + 0.00637 s + 0.307 \times 10^{-4}}, \quad (15)$$

$$\Sigma_4(s) = \frac{\phi}{\phi_d} = \frac{0.611 \times 10^{-16} s + 0.483 \times 10^{-4}}{s^2 + 0.01231 s + 0.521 \times 10^{-4}}, \quad (16)$$

$$\Sigma_5(s) = \frac{\theta}{\theta_d} = \frac{0.762 \times 10^{-13} s + 0.568 \times 10^{-4}}{s^2 + 0.01357 s + 0.585 \times 10^{-4}}, \quad (17)$$

$$\Sigma_6(s) = \frac{\psi}{\psi_d} = \frac{0.142 \times 10^{-13} s + 0.149 \times 10^{-3}}{s^2 + 0.00319 s + 0.133 \times 10^{-3}}. \quad (18)$$

The equations (13)–(18) together describe the SMC-linearised tricopter dynamics in closed-loop having six outputs and inputs.

IV. 'Mixed' NI plus Passivity-based cooperative control of a multi-tilt tricopter system

We will now dive into another key result of this paper. Here we will develop a simple but easy-to-implement cooperative control scheme (shown in Fig. 3) for a fleet of SMC-linearised tricopter drones exploiting the idea of a distributed 'mixed' SNI + strictly Passive controller.

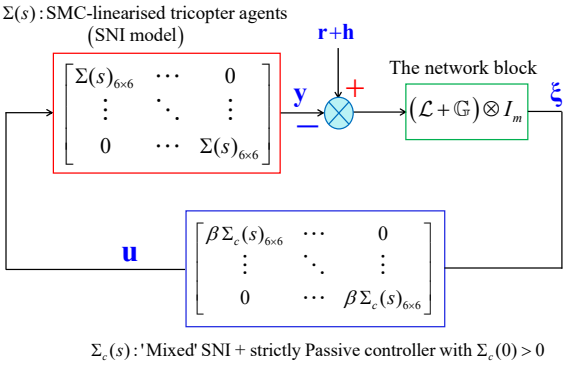

Fig. 3: A formation tracking scheme for a multi-tricopter system $\Sigma(s)$ which exhibit SNI property using a distributed 'mixed' SNI + strictly Passive controller $\Sigma_c(s)$.

Theorem 2: Consider a homogeneous multi-tricopter system whose SMC-linearised model $\Sigma(s)$, as derived in (13)–(18), has a (6×6) SNI transfer function matrix. Let the communication topology $\mathscr{G}$ satisfy Property 1. Let $\mathbf{r} = \big[\boldsymbol{r}_1^\top \ \boldsymbol{r}_2^\top, \ldots, \boldsymbol{r}_N^\top\big]^\top$ denote the reference vector and $\mathbf{h} = \big[\boldsymbol{h}_1^\top \ \boldsymbol{h}_2^\top, \ldots, \boldsymbol{h}_N^\top\big]^\top$ represent the desired formation configuration vector. If a 'mixed' SNI + strictly Passive controller $\Sigma_c(s) \in \mathscr{RH}_\infty^{6\times 6}$ with $\Sigma_c(0) > 0$ is used as in Fig. 3. Then, there always exists a finite $\beta \in (0, \beta^\star]$ such that the proposed scheme in Fig. 3 drives all agents to converge to the state trajectory of the leader agent and the agents asymptotically reach the desired formation, under the influence of the following 'mixed' SNI + strictly Passive distributed controller

$$\mathbf{u}_i = \beta \Sigma_c(s) \sum_{j=1}^{N} w_{ij}\big((\mathbf{y}_i - \mathbf{h}_i) - (\mathbf{y}_j - \mathbf{h}_j)\big) + w_{0,i}(\mathbf{h}_i + \mathbf{r}_i - \mathbf{y}_i) \quad \forall i \in \{1, 2, \ldots, N\}. \quad (19)$$

Proof. The proof has been divided into two major parts. Part 1 derives the closed-loop asymptotic stability of the proposed cooperative control scheme shown in Fig. 3 and Part 2 shows that the consensus (or formation) error of the agents decays to zero.

Part 1: Let $\bar{\lambda}_i(s)$ be the characteristic loci of the transfer function mapping $[(\mathscr{L} + \mathbb{P}_G) \otimes \Sigma_c(s)\Sigma(s)]$ of the networked loop shown in Fig. 3. To proceed with the proof exploiting the characteristic loci technique, we define two sets of the Laplace variable s, $\Psi_{\pm j}$ and Ψ_∞, as marked in the s-plane D-contour shown in Fig. 4a. From Theorem 1, the closed-loop interconnection (in negative feedback) of $[I_n \otimes \Sigma(s)]$ and $[(\mathscr{L} + \mathbb{P}_G) \otimes \beta\Sigma_c(s)]$, like in Fig. 3, is asymptotically stable as far as none of the $\bar{\lambda}_i(j\omega)$ encircles the $(-\frac{1}{\beta} + j0)$ point for any $\beta \in (0, \beta^\star]$. This condition is graphically illustrated through Fig. 4b, that is, all $\bar{\lambda}_i(j\omega)$ completely remain inside the Cyan-coloured region. In the following proof, the index $i \in \{1, 2, \ldots, nm\}$ will be uniformly used.

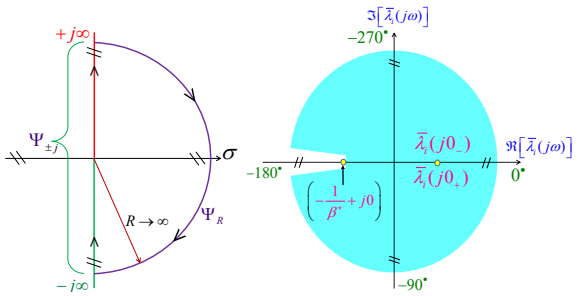

Fig. 4: (a) The s-plane Nyquist $\mathscr{D}$-contour; and (b) All $\bar{\lambda}_i(j\omega)$ of $(\mathscr{L}+\mathbb{P}_G)\otimes\Sigma_c(s)\Sigma(s)$ remain inside the Cyan-coloured region when $\Sigma(s)$ is SNI and $\Sigma_c(s)$ is 'mixed' SNI + strictly Passive with $\Sigma(0)>0$ and $\Sigma_c(0)>0$.

Step 1: For the subset $s\in\Psi_{\pm j}\cup\{0\}$

We suppose $\lambda_i\left[(\mathscr{L}+\mathbb{P}_G)\otimes\Sigma_c(j\omega)\Sigma(j\omega)\right] = \lambda_i\left[(\mathscr{L}+\mathbb{P}_G)\right]\ |n_i(j\omega)||g_i(j\omega)|e^{j(\psi_i+\phi_i)}$ at every value of $\omega\in(0,\infty)$ where the symbol $\lambda_i[\cdot]$ denotes simply the eigenvalues of a matrix. Then, $\psi_i(\omega)\in[-\pi,0]$ and $\phi_i(\omega)\in(-\pi,\frac{\pi}{2})$ for all $\omega\in(0,\infty)$ and for all i because $\Sigma(s)$ is stable NI and $\Sigma_c(s)$ is 'mixed' SNI + strictly Passive and thus, $\angle\bar{\lambda}_i(j\omega)=(\psi_i(\omega)+\phi_i(\omega))\in[-2\pi,0]$ for all $\omega\in(0,\infty)$ and for all i. In a similar fashion, for all $\omega\in(-\infty,0)$, $\angle\bar{\lambda}_i(j\omega)\in[-2\pi,0]$. From Property 1, it follows that at $\omega=0$, $\bar{\lambda}_i\left[(\mathscr{L}+\mathbb{P}_G)\otimes\Sigma_c(0)\Sigma(0)\right] = \bar{\lambda}_i\left[(\mathscr{L}+\mathbb{P}_G)\right]|n_i(0)||g_i(0)|\angle 0$ since $\Sigma_c(0)>0$, $\Sigma(0)>0$ and $(\mathscr{L}+\mathbb{P}_G)>0$. Thus, since neither $\Sigma_c(s)$ nor $\Sigma(s)$ have poles at $s=0$ (the origin), the points $\bar{\lambda}_i(j0_-)$ and $\bar{\lambda}_i(j0_+)$ (zero-frequency points) of all $\bar{\lambda}_i(s)$ coincide and lie on the positive real axis of the characteristic loci plane. Furthermore, none of the characteristic loci $\lambda_i(j\omega)$ crosses the positive or negative real axis at infinite distance when $s\in\Psi_{\pm j}\cup\{0\}$ since both $\Sigma_c(s)$ and $\Sigma(s)$ have no poles at $s=0$. This implies that when $s\in\Psi_{\pm j}\cup\{0\}$, the magnitude of the angle $\angle\bar{\lambda}_i(j\omega)$ contributed by each of $\bar{\lambda}_i(s)$ lies in the range $[-2\pi,0]$ for all $\omega\in\mathbb{R}$. Most essentially, as there is no infinite crossover on the negative real axis and $\bar{\lambda}_i\left[\Sigma_c(0)\Sigma(0)\right]>0\ \forall i$, we can always choose a finite $\beta^\star$ for which even the worst-case critical point $\left(-\frac{1}{\beta^\star}+j0\right)$ is never encircled by any $\bar{\lambda}_i(s)$.

Step 2: For the subset $s\in\Psi_\infty$

Like $\bar{\lambda}_i(j0_-)$ and $\bar{\lambda}_i(j0_+)$, the points at $\omega=\infty$ denoted by $\bar{\lambda}_i(+j\infty)$ and $\bar{\lambda}_i(-j\infty)$ can be expressed as $\bar{\lambda}_i\left[(\mathscr{L}+\mathbb{P}_G)\otimes\Sigma_c(\infty)\Sigma(\infty)\right] = \bar{\lambda}_i\left[(\mathscr{L}+\mathbb{P}_G)\right]|n_i(\infty)|\ |g_i(\infty)|\angle\left(\psi_i(\infty)+\phi_i(\infty)\right)\forall i\in\{1,2,\ldots,nm\}$. These infinite frequency points coincide and lie either at the origin on the positive/negative real axis at finite distances from the origin as in the present scenario $\lambda_i[\Sigma_c(\infty)\Sigma(\infty)]\in\mathbb{R}\ \forall i$ and $(\mathscr{L}+\mathbb{P}_G)>0$.

Depending on Step 1 and Step 2, we can conclude that all $\bar{\lambda}_i(s)$ remain inside the Cyan-coloured region (in Fig. 4b) which guarantees that even the worst-case critical point $(-\frac{1}{\beta^\star}+j0)$ will remain unencircled by all the characteristic loci. This means that the proposed cooperative control scheme remains asymptotically stable for a finite range of $\beta>0$.

Part 2: Since the networked closed-loop system shown in Fig. 3 is asymptotically stable (as derived in Part 1), the formation tracking (or consensus reaching) error will asymptotically decay to zero. In a notational expression, $\lim_{t\to\infty}\xi_i(t)=0$ or $\lim_{t\to\infty}[\mathbf{r}_i(t)+\mathbf{h}_i(t)-\mathbf{y}_i(t)]=0\ \forall i$. This part naturally results from [28, Theorem 1]. Consequently, we can infer that the linearised multi-tricopter system will attain the desired formation (or consensus) specified by $\mathbf{r}$ and $\mathbf{h}$. ■

V. Case Study and Simulation Results

We consider a fleet of six identical tricopter drones and the control objective is to attain a predefined time-varying formation and keep tracking the target (or the leader). According to the proposed cooperative control scheme, we choose a (6×6) 'mixed' SNI + strictly Passive controller transfer function matrix, in which i) $n_1(s)=\frac{10^7}{(s+\rho_1)}$ is a high-gain SNI controller required for controlling the x axis; ii) a set of three SNI controllers $n_j(s)=\frac{120}{(s+5)(s+\rho_j)}\ \forall j\in\{4,5,6\}$ for the roll, pitch and yaw axes respectively; and iii) a couple of high-gain strictly Passive controllers $n_j(s)=\frac{(8\times 10^7)(s+2)}{(s+\rho_j)}\ \forall j\in\{2,3\}$ for the y and z axes respectively, where $\left[\rho_1,\ \rho_2,\ \rho_3,\ \rho_4,\ \rho_5,\ \rho_6\right]=\left[15,100,80,90,20,30\right]$. The formation reference (or the target positions) is set as $\mathbf{r}_{i_1}=\left[4\ \ 3\ \ 2\ \ \mathbf{0}_3^\top\right]^\top\ \forall t<10$s and $\mathbf{r}_{i_2}=\left[-1\ \ 5\ \ 3.2\ \ \mathbf{0}_3^\top\right]^\top\ \forall t\geq 10$s and $\forall i\in\{1,2,\ldots,6\}$ where $\mathbf{0}_3=\left[0\ 0\ 0\right]^\top$. The formation configuration vectors $\mathbf{h}_i$ for the multi-tilt tricopters are chosen as $\boldsymbol{h}_i=\begin{bmatrix}\gamma_i\cos(\theta_i)\\ \gamma_i\sin(\theta_i)\\ 0\\ \mathbf{0}_3\end{bmatrix}$ where $\theta_i=\left[\pi/4,2\pi/4,3\pi/4,\pi,3\pi/2,2\pi\right]$ for all $i\in\{1,2,\ldots,6\}$ and all $t<10$s. Whereas for $t\geq 10$s, $\boldsymbol{h}_i=\begin{bmatrix}\beta_i\cos(\frac{(2i+1)\pi}{6})\\ \beta_i\sin(\frac{(2i+1)\pi}{6})\\ 0\\ \mathbf{0}_3\end{bmatrix}$. Note the formation radius $\delta=2.0$m and $\gamma_i=\delta\ \forall i\in\{1,3,5\}$, $\gamma_i=\frac{2\delta}{3}\ \forall i\in\{2,6\}$ and $\gamma_4=\delta/2$. Similarly, $\beta_i=\delta\ \forall i\in\{1,2,4,5\}$ and $\beta_i=\delta/2\ \forall i\in\{3,6\}$. During the first phase (for $t<10$ seconds), the tricopter agents form a four-sided shape similar to a triangle around the target and in the next phase (for $t\geq 10$seconds), they form a double echelon-like formation surrounding the target, and noting the change in the formation reference from $\mathbf{r}_{i_1}$ to $\mathbf{r}_{i_2}$ at $t=10$ seconds. It can be noted from Fig. 5 that the six tricopters achieve leader-following formation tracking (implying consensus is also achieved) as t tends to infinity ($t\to\infty$). It is worth mentioning that despite the changes in $\mathbf{r}_i$ and $\mathbf{h}_i$, the stability of the overall network is maintained and the tricopters achieved the new formation successfully.

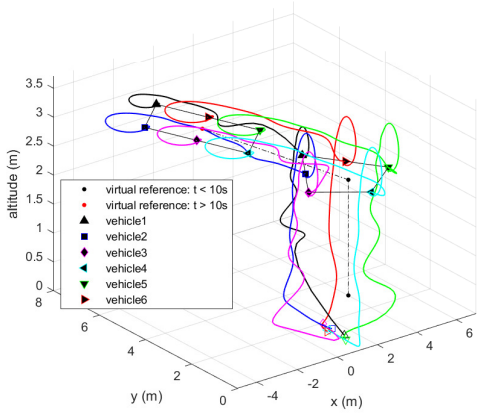

Fig. 5: Formation tracking of six tricopter agents by the proposed cooperative control scheme: Formation configuration after 10sec.

VI. Conclusions

This paper considers the cooperative control problem of a group of tricopter drones connected via a network. A continuous-time system identification algorithm is developed to identify a custom-made multi-tilt tricopter model in a closed loop that enforces the Negative Imaginary (NI) property. Sliding-mode Control (SMC) strategy has been used to linearise the highly-coupled and nonlinear dynamics of the tricopters. We then proposed a simple yet effective and easy-to-implement cooperative control scheme for a class of multi-tricopter systems that exhibits NI property upon applying an SMC-based linearisation technique in the inner loop. The theoretical proof of this scheme relies on the characteristic loci theory in contrast to the typical Lyapunov-based approaches found in the cooperative control literature. A detailed Matlab simulation case study is also provided to validate the effectiveness of the proposed scheme.

References

[1] R. Mahony, V. Kumar, and P. Corke, "Multirotor aerial vehicles: Modeling, estimation, and control of quadrotor," *IEEE Robotics & Automation Magazine*, vol. 19, no. 3, pp. 20–32, Sep 2012.

[2] M. Senanayake, I. Senthooran, J. C. Barca, H. Chung, J. Kamruzzaman, and M. Murshed, "Search and tracking algorithms for swarms of robots: A survey," *Robotics and Autonomous Systems*, vol. 75, pp. 422–434, Jan 2016.

[3] A. Shukla and H. Karki, "Application of robotics in onshore oil and gas industry – A review Part I," *Robotics and Autonomous Systems*, vol. 75, pp. 490–507, Jan 2016.

[4] A. Lanzon and I. R. Petersen, "Stability robustness of a feedback interconnection of systems with negative imaginary frequency response," *IEEE Transactions on Automatic Control*, vol. 53, no. 4, pp. 1042–1046, May 2008.

[5] B. Bhikkaji, S. O. Reza Moheimani, and I. R. Petersen, "A negative imaginary approach to modeling and control of a collocated structure," *IEEE/ASME Transactions on Mechatronics*, vol. 17, no. 4, pp. 717–727, Aug 2012.

[6] S. Kurawa, P. Bhowmick, and A. Lanzon, "Dynamic output feedback controller synthesis using an lmi-based α-strictly negative imaginary framework," in *Proceedings of 27th Mediterranean Conference on Control and Automation*, July 2019, pp. 81–86.

[7] N. Nikooienejad and S. O. Reza Moheimani, "Convex synthesis of SNI controllers based on frequency-domain data: MEMS nanopositioner example," *IEEE Transactions on Control Systems Technology*, vol. 30, no. 2, pp. 767–778, March 2022.

[8] C. Li, J. Wang, J. Shan, A. Lanzon, and I. R. Petersen, "Robust cooperative control of networked train platoons: A negative-imaginary systems' perspective," *IEEE Transactions on Control of Network Systems*, vol. 8, no. 4, pp. 1743–1753, Dec 2021.

[9] A. Lanzon and P. Bhowmick, "Characterisation of input-output negative imaginary systems in a dissipative framework," *IEEE Transactions on Automatic Control*, vol. 68, pp. 959–974, Feb 2023.

[10] S. Kurawa, P. Bhowmick, and A. Lanzon, "Negative imaginary theory for a class of linear time-varying systems," *IEEE Control Systems Letters*, vol. 5, no. 3, pp. 1001–1006, 2021.

[11] P. Bhowmick and A. Lanzon, "Applying negative imaginary systems theory to non-square systems with polytopic uncertainty," *Automatica*, vol. 128, pp. 1–14, June 2021.

[12] P. Bhowmick and S. Patra, "On LTI output strictly negative-imaginary systems," *Systems & Control Letters*, vol. 100, pp. 32–42, Feb 2017.

[13] P. Bhowmick and A. Lanzon, "Output strictly negative imaginary systems and its connections to dissipativity theory," in *Proceedings of 58th IEEE Conference on Decision and Control*, Dec 2019, pp. 6754–6759.

[14] P. Bhowmick and A. Lanzon, "Time-domain output negative imaginary systems and its connection to dynamic dissipativity," in *Proceedings of 59th IEEE Conference on Decision and Control*, Dec 2020, pp. 5167–5172.

[15] V. P. Tran, M. A. Garratt, and I. R. Petersen, "Switching time-invariant formation control of a collaborative multi-agent system using negative imaginary systems theory," *Control Engineering Practice*, vol. 95, no. 104245, pp. 1–16, Nov 2020.

[16] M. Kara-Mohamed and A. Lanzon, "Design and control of novel tri-rotor UAV," in *Proceedings of UKACC International Conference on Control*, Cardiff, UK, Sep 2012, pp. 304–309.

[17] B. L. Stevens, F. L. Lewis, and E. N. Johnson, *Aircraft Control and Simulation: Dynamics, Controls Design, and Autonomous Systems*. Hoboken, New Jersey: John Wiley and Sons, 2015.

[18] C. Desoer and M. Vidyasagar, *Feedback Systems: Input-Output Properties*, ser. Classics in Applied Mathematics. Society for Industrial and Applied Mathematics, 2009.

[19] A. Lanzon and H.-J. Chen, "Feedback stability of negative imaginary systems," *IEEE Transactions on Automatic Control*, vol. 62, no. 11, pp. 5620–5633, Nov 2017.

[20] A. G. J. Macfarlane and J. J. Belletrutti, "The characteristic locus design method," *Automatica*, vol. 9, no. 5, pp. 575–588, 1973.

[21] J. Wang, A. Lanzon, and I. R. Petersen, "Robust output feedback consensus for networked negative-imaginary systems," *IEEE Transactions on Automatic Control*, vol. 60, no. 9, pp. 2547–2552, Sep. 2015.

[22] J. Hu, B. Lennox, and F. Arvin, "Robust formation control for networked robotic systems using negative imaginary dynamics," *under review in Automatica*, pp. 1–13, 2021.

[23] P. Bhowmick, A. Ganguly, and S. Sen, "A new consensus-based formation tracking scheme for a class of robotic systems using negative imaginary property," *IFAC-PapersOnLine*, vol. 55, no. 1, pp. 685–690, May 2022.

[24] P. Bhowmick and S. Patra, "On decentralized integral controllability of stable negative-imaginary systems and some related extensions," *Automatica*, vol. 94, pp. 443–451, Aug 2018.

[25] P. Bhowmick, S. Bhadra, and A. Panda, "A two-loop group formation tracking control scheme for networked tri-rotor UAVs using an ARE-based approach," *in press Asian Journal of Control*, pp. 1–16, May 2022, DOI:10.1002/asjc.2722.

[26] H. K. Khalil, *Nonlinear Systems*, 3rd ed. Englewood Cliffs, New Jersey, USA: Prentice-Hall, 2002.

[27] R. Mohd-Mokhtar and L. Wang, "Continuous time state space model identification using closed-loop data," in *2nd IEEE Asia International Conference on Modelling Simulation*, May 2008, pp. 812–817.

[28] J. H. Seo, H. Shim, and J. Back, "Consensus of high-order linear systems using dynamic output feedback compensator: Low gain approach," *Automatica*, vol. 45, no. 11, pp. 2659–2664, 2009.